Chapter 6

Lyapunov exponents

LET US APPLY our newly acquired tools to the fundamental diagnostics in dynamics: Is a given system 'chaotic'? And if so, how chaotic? If all points in a neighborhood of a trajectory converge toward the same orbit, the attractor is a fixed point or a limit cycle. However, if the attractor is strange, any two trajectories $x(t) = f^t(x_0)$ and $x(t)+\delta x(t) = f^t(x_0+\delta x_0)$ that start out very close to each other separate exponentially with time, and in a finite time their separation attains the size of the accessible state space.

example 2.3

section 1.3.1

remark 6.1

This *sensitivity to initial conditions* can be quantified as

$$\|\,\delta x(t)\,\| \approx e^{\lambda t}\,\|\,\delta x_0\,\| \tag{6.1}$$

where λ, the mean rate of separation of trajectories of the system, is called the leading *Lyapunov exponent*. In the limit of infinite time the Lyapunov exponent is a global measure of the rate at which nearby trajectories diverge, averaged over the strange attractor. As it so often goes with easy ideas, it turns out that Lyapunov exponents are not natural for study of dynamics, and we would have passed them over in silence, were it not for so much literature that talks about them. So in a textbook we are duty bound to explain what all the excitement is about. But then we round the chapter off with a scholarly remark almost as long as the chapter itself: we do not recommend that you evaluate Lyapunov exponents and Lyapunov singular vectors. Compute the stability exponents / covariant vectors.

6.1 Stretch, strain and twirl

Diagonalizing the matrix: that's the key to the whole thing.
— Governor Arnold Schwarzenegger

In general the Jacobian matrix J is neither diagonal, nor diagonalizable, nor con-

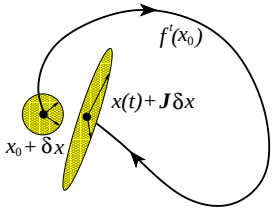

Figure 6.1: The linearized flow maps a swarm of initial points in an infinitesimal spherical neighborhood of squared radius δx^2 at x_0 into an ellipsoid $\delta x^\top (J^\top J)\,\delta x$ at $x(t)$ a finite time t later, rotated and stretched/compressed along the principal axes by streches $\{\sigma_j\}$.

stant along the trajectory. What is a geometrical meaning of the mapping of a neighborhood by J? Here the continuum mechanics insights are helpful, in particular the polar decomposition which affords a visualization of the linearization of a flow as a mapping of the initial ball into an ellipsoid (figure 6.1).

First, a few definitions: A symmetric $[d\times d]$ matrix Q is *positive definite*, $Q > 0$, if $x^\top Q x > 0$ for any nonzero vector $x \in \mathbb{R}^d$. Q is *negative definite*, $Q < 0$, if $x^\top Q x < 0$ for any nonzero vector x. Alternatively, Q is a positive (negative) definite matrix if all its eigenvalues are positive (negative). A matrix R is orthogonal if $R^\top R = \mathbf{1}$, and proper orthogonal if $\det R = +1$. Here the superscript $^\top$ denotes the transpose. For example, $(x_1,\cdots,x_d)$ is a row vector, $(x_1,\cdots,x_d)^\top$ is a column vector.

By the polar decomposition theorem, a deformation J can be factored into a rotation R and a right / left stretch tensor U / V,

remark 6.2

$$J = RU = VR\,, \tag{6.2}$$

where R is a proper-orthogonal matrix and U, V are symmetric positive definite matrices with strictly positive real eigenvalues $\{\sigma_1,\sigma_2,\cdots,\sigma_d\}$ called *principal stretches* (singular values, Hankel singular values), and with orthonormal eigenvector bases,

$$\begin{aligned} U\,u^{(i)} &= \sigma_i u^{(i)}\,, \qquad \{u^{(1)},u^{(2)},\cdots,u^{(d)}\} \\ V\,v^{(i)} &= \sigma_i v^{(i)}\,, \qquad \{v^{(1)},v^{(2)},\cdots,v^{(d)}\}\,. \end{aligned} \tag{6.3}$$

$\sigma_i > 1$ for stretching and $0 < \sigma_i < 1$ for compression along the direction $u^{(i)}$ or $v^{(i)}$. $\{u^{(j)}\}$ are the *principal axes of strain* at the initial point x_0; $\{v^{(j)}\}$ are the principal axes of strain at the present placement x. From a geometric point of view, J maps the unit sphere into an ellipsoid, figure 6.1; the principal stretches are then the lengths of the semiaxes of this ellipsoid. The rotation matrix R carries the initial axes of strain into the present ones, $V = RUR^\top$. The eigenvalues of the

remark 6.1

$$\begin{aligned} \text{right Cauchy-Green strain tensor:} &\quad J^\top J = U^2 \\ \text{left Cauchy-Green strain tensor:} &\quad J\,J^\top = V^2 \end{aligned} \tag{6.4}$$

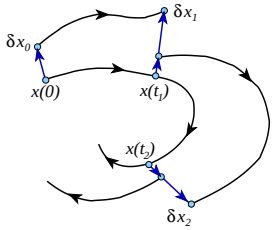

Figure 6.2: A long-time numerical calculation of the leading Lyapunov exponent requires rescaling the distance in order to keep the nearby trajectory separation within the linearized flow range.

are $\{\sigma_j^2\}$, the squares of principal stretches.

example 6.2
p. 120

6.2 Lyapunov exponents

(J. Mathiesen and P. Cvitanović)

The mean growth rate of the distance $\|\delta x(t)\| / \|\delta x_0\|$ between neighboring trajectories (6.1) is given by the leading *Lyapunov exponent* which can be estimated for long (but not too long) time t as

$$\lambda \simeq \frac{1}{t} \ln \frac{\|\delta x(t)\|}{\|\delta x(0)\|} \tag{6.5}$$

For notational brevity we shall often suppress the dependence of quantities such as $\lambda = \lambda(x_0, t)$, $\delta x(t) = \delta x(x_0, t)$ on the initial point x_0. One can use (6.5) as is, take a small initial separation δx_0, track the distance between two nearby trajectories until $\|\delta x(t_1)\|$ gets significantly big, then record $t_1\lambda_1 = \ln(\|\delta x(t_1)\| / \|\delta x_0\|)$, rescale $\delta x(t_1)$ by factor $\delta x_0/\delta x(t_1)$, and continue add infinitum, as in figure 6.2, with the leading Lyapunov exponent given by

$$\lambda = \lim_{t\to\infty} \frac{1}{t} \sum_i t_i \lambda_i \,, \qquad t = \sum_i t_i \,. \tag{6.6}$$

Deciding what is a safe 'linear range', the distance beyond which the separation vector $\delta x(t)$ should be rescaled, is a dark art.

We can start out with a small δx and try to estimate the leading Lyapunov exponent λ from (6.6), but now that we have quantified the notion of linear stability in chapter 4, we can do better. The problem with measuring the growth rate of the distance between two points is that as the points separate, the measurement is less and less a local measurement. In the study of experimental time series this might

be the only option, but if we have equations of motion, a better way is to measure the growth rate of vectors transverse to a given orbit.

Given the equations of motion, for infinitesimal δx we know the $\delta x_i(t)/\delta x_j(0)$ ratio exactly, as this is by definition the Jacobian matrix

$$\lim_{\delta x(0)\to 0} \frac{\delta x_i(t)}{\delta x_j(0)} = \frac{\partial x_i(t)}{\partial x_j(0)} = J^t_{ij}(x_0) \,,$$

so the leading Lyapunov exponent can be computed from the linearization (4.16)

$$\lambda(x_0) = \lim_{t\to\infty} \frac{1}{t} \ln \frac{\left\| J^t(x_0)\,\delta x_0 \right\|}{\|\,\delta x_0\,\|} = \lim_{t\to\infty} \frac{1}{2t} \ln\left(\hat{n}^\top J^{t\top} J^t \hat{n}\right) . \tag{6.7}$$

In this formula the scale of the initial separation drops out, only its orientation given by the initial orientation unit vector $\hat{n} = \delta x_0 / \|\delta x_0\|$ matters. If one does not care about the orientation of the separation vector between a trajectory and its perturbation, but only its magnitude, one can interpret $\left\| J^t \delta x_0 \right\|^2 = \delta x_0{}^\top (J^{t\top} J^t)\,\delta x_0$, as the *error correlation matrix*. In the continuum mechanics language, the right Cauchy-Green strain tensor $J^\top J$ (6.4) is the natural object to describe how linearized neighborhoods deform. In the theory of dynamical systems the *stretches* of continuum mechanics are called the *finite-time Lyapunov* or *characteristic* exponents,

$$\lambda(x_0, \hat{n}; t) = \frac{1}{t} \ln \left\| J^t \hat{n} \right\| = \frac{1}{2t} \ln\left(\hat{n}^\top J^{t\top} J^t \hat{n}\right) . \tag{6.8}$$

They depend on the initial point x_0 and on the direction of the unit vector $\hat{n}$, $\|\,\hat{n}\,\| = 1$ at the initial time. If this vector is aligned along the ith principal stretch, $\hat{n} = u^{(i)}$, then the corresponding finite-time Lyapunov exponent (rate of stretching) is given by

$$\lambda_j(x_0; t) = \lambda(x_0, u^{(j)}; t) = \frac{1}{t} \ln \sigma_j(x_0; t). \tag{6.9}$$

We do not need to compute the strain tensor eigenbasis to determine the leading *Lyapunov exponent*,

$$\lambda(x_0, \hat{n}) = \lim_{t\to\infty} \frac{1}{t} \ln \left\| J^t \hat{n} \right\| = \lim_{t\to\infty} \frac{1}{2t} \ln\left(\hat{n}^\top J^{t\top} J^t \hat{n}\right) , \tag{6.10}$$

as expanding the initial orientation in the strain tensor eigenbasis (6.3), $\hat{n} = \sum(\hat{n} \cdot u^{(i)})u^{(i)}$, we have

$$\hat{n}^\top J^{t\top} J^t \hat{n} = \sum_{i=1}^{d} (\hat{n} \cdot u^{(i)})^2 \sigma_i^2 = (\hat{n} \cdot u^{(1)})^2 \sigma_1^2 \left(1 + O(\sigma_2^2/\sigma_1^2)\right) ,$$

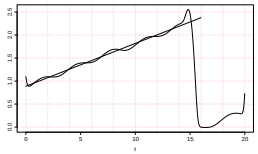

Figure 6.3: A numerical computation of the logarithm of the stretch $\hat{n}^\top (J^{t\top} J^t)\hat{n}$ in formula (6.10) for the Rössler flow (2.23), plotted as a function of the Rössler time units. The slope is the leading Lyapunov exponent $\lambda \approx 0.09$. The exponent is positive, so numerics lends credence to the hypothesis that the Rössler attractor is chaotic. The big unexplained jump illustrates perils of Lyapunov exponents numerics. (J. Mathiesen)

with stretches ordered by decreasing magnitude, $\sigma_1 > \sigma_2 \geq \sigma_3 \cdots$. For long times the largest stretch dominates exponentially in (6.10), provided the orientation $\hat{n}$ of the initial separation was not chosen perpendicular to the dominant expanding eigen-direction $u^{(1)}$. Furthermore, for long times $J^t\hat{n}$ is dominated by the largest stability multiplier Λ_1, so the leading Lyapunov exponent is

$$\begin{aligned} \lambda(x_0) &= \lim_{t\to\infty} \frac{1}{t} \left\{ \ln \left\| \hat{n} \cdot \mathbf{e}^{(1)} \right\| + \ln|\Lambda_1(x_0,t)| + O(e^{-2(\lambda_1-\lambda_2)t}) \right\} \\ &= \lim_{t\to\infty} \frac{1}{t} \ln|\Lambda_1(x_0,t)|\,, \end{aligned} \tag{6.11}$$

where $\Lambda_1(x_0,t)$ is the leading eigenvalue of $J^t(x_0)$. The leading Lyapunov exponent now follows from the Jacobian matrix by numerical integration of (4.10). The equations can be integrated accurately for a finite time, hence the infinite time limit of (6.7) can be only estimated from a finite set of evaluations of $\frac{1}{2}\ln(\hat{n}^\top J^{t\top} J^t \hat{n})$ as function of time, such as figure 6.3 for the Rössler flow (2.23).

As the local expansion and contraction rates vary along the flow, the temporal dependence exhibits small and large humps. The sudden fall to a low value in figure 6.3 is caused by a close passage to a folding point of the attractor, an illustration of why numerical evaluation of the Lyapunov exponents, and proving the very existence of a strange attractor is a difficult problem. The approximately monotone part of the curve you can use (at your own peril) to estimate the leading Lyapunov exponent by a straight line fit.

As we can already see, we are courting difficulties if we try to calculate the Lyapunov exponent by using the definition (6.11) directly. First of all, the state space is dense with atypical trajectories; for example, if x_0 happens to lie on a periodic orbit p, λ would be simply $\ln|\sigma_{p,1}|/T_p$, a local property of cycle p, not a global property of the dynamical system. Furthermore, even if x_0 happens to be a 'generic' state space point, it is still not obvious that $\ln|\sigma_{p,1}(x_0,t)|/t$ should be converging to anything in particular. In a Hamiltonian system with coexisting elliptic islands and chaotic regions, a chaotic trajectory gets captured in the neighborhood of an elliptic island every so often and can stay there for arbitrarily long time; as there the orbit is nearly stable, during such episode $\ln|\sigma_{p,1}(x_0,t)|/t$ can dip arbitrarily close to 0^+. For state space volume non-preserving flows the trajectory can traverse locally contracting regions, and $\ln|\sigma_{p,1}(x_0,t)|/t$ can occasionally go negative; even worse, one never knows whether the asymptotic attractor is periodic or 'chaotic', so any finite time estimate of λ might be dead wrong. exercise 6.3

Résumé

Let us summarize the 'stability' chapters 4 to 6. A neighborhood of a trajectory deforms as it is transported by a flow. In the linear approximation, the stability matrix A describes the shearing / compression / expansion of an infinitesimal neighborhood in an infinitesimal time step. The deformation after a finite time t is described by the Jacobian matrix J^t, whose eigenvalues (stability multipliers) depend on the choice of coordinates.

Floquet multipliers and *eigen-vectors* are intrinsic, invariant properties of finite-time, compact invariant solutions, such as periodic orbits and relative periodic orbits; they are explained in chapter 5. *Stability exponents* [6.1] are the corresponding long-time limits estimated from typical ergodic trajectories.

Finite-time Lyapunov exponents and the associated *principal axes* are defined in (6.8). Oseledec *Lyapunov exponents* are the $t \to \infty$ limit of these.

Commentary

Remark 6.1 Lyapunov exponents are uncool, and ChaosBook does not use them at all. Eigenvectors / eigenvalues are suited to study of iterated forms of a matrix, such as Jacobian matrix J^t or exponential $\exp(tA)$, and are thus a natural tool for study of dynamics. Principal vectors are not, they are suited to study of the matrix J^t itself. The polar (singular value) decomposition is convenient for numerical work (any matrix, square or rectangular, can be brought to such form), as a way of estimating the effective rank of matrix J by separating the large, significant singular values from the small, negligible singular values.

Lorenz [6.2, 6.3, 6.4] pioneered the use of singular vectors in chaotic dynamics. We found the Goldhirsch, Sulem and Orszag [6.1] exposition very clear, and we also enjoyed Hoover and Hoover [6.5] pedagogical introduction to computation of Lyapunov spectra by the method of Lagrange multipliers. Greene and Kim [6.6] discuss singular values vs. Jacobian matrix eigenvalues. While they conclude that "singular values, rather than eigenvalues, are the appropriate quantities to consider when studying chaotic systems," we beg to differ: their Fig. 3, which illustrates various semiaxes of the ellipsoid in the case of Lorenz attractor, as well as the figures in ref. [6.7], are a persuasive argument for *not* using singular values. The covariant vectors are tangent to the attractor, while the principal axes of strain point away from it. It is the perturbations within the attractor that describe the long-time dynamics; these perturbations lie within the subspace spanned by the leading covariant vectors.

That is the first problem with Lyapunov exponents: stretches $\{\sigma_j\}$ are *not related* to the Jacobian matrix J^t eigenvalues $\{\Lambda_j\}$ in any simple way. The eigenvectors $\{u^{(j)}\}$ of strain tensor $J^\top J$ that determine the orientation of the principal axes, are distinct from the Jacobian matrix eigenvectors $\{\mathbf{e}^{(j)}\}$. The strain tensor $J^\top J$ satisfies no multiplicative semigroup property such as (4.20); unlike the Jacobian matrix (5.3), the strain tensor $J^{\top r} J^r$ for the rth repeat of a prime cycle p is not given by a power of $J^\top J$ for the single traversal of the prime cycle p. Under time evolution the covariant vectors map forward as $\mathbf{e}^{(j)} \to J\,\mathbf{e}^{(j)}$ (transport of the velocity vector (4.9) is an example). In contrast, the principal axes have to be recomputed from the scratch for each time t.

If Lyapunov exponents are not dynamical, why are they invoked so frequently? One reason is fear of mathematics: the monumental and therefore rarely read Oseledec [6.8, 6.9] Multiplicative Ergodic Theorem states that the limits (6.7–6.11) exist for almost all points x_0 and vectors $\hat{n}$, and that there are at most d distinct Lyapunov exponents $\lambda_i(x_0)$ as $\hat{n}$ ranges over the tangent space. To intimidate the reader further we note in passing that "moreover there is a fibration of the tangent space $\mathbf{T}_x\mathcal{M}$, $L^1(x) \subset L^2(x) \subset \cdots \subset L^r(x) = \mathbf{T}_x\mathcal{M}$, such that if $\hat{n} \in L^i(x) \setminus L^{i-1}(x)$ the limit (6.7) equals $\lambda_i(x)$." Oseledec proof is important mathematics, but the method is not helpful in elucidating dynamics.

The other reason to study singular vectors is physical and practical: Lorenz [6.2, 6.3, 6.4] was interested in the propagation of errors, i.e., how does a cloud of initial points $x(0) + \delta x(0)$, distributed as a Gaussian with covariance matrix $Q(0) = \langle \delta x(0)\, \delta x(0)^\top \rangle$, evolve in time? For linearized flow with initial isotropic distribution $Q(0) = \epsilon \mathbf{1}$ the answer is given by the left Cauchy-Green strain tensor,

$$Q(t) = \left\langle \delta x(0)\, J\, J^\top \delta x(0)^\top \right\rangle = J\, Q(t)\, J^\top = \epsilon\, J\, J^\top . \tag{6.12}$$

The deep problem with Lyapunov exponents is that the intuitive definition (6.5) depends on the notion of distance $\| \delta x(t) \|$ between two state space points. The Euclidean (or L^2) distance is natural in the theory of $3D$ continuous media, but what the norm should be for other state spaces is far from clear, especially in high dimensions and for PDEs. As we have shown in sect. 5.3, Floquet multipliers are invariant under all local smooth nonlinear coordinate transformations, they are intrinsic to the flow, and the Floquet eigenvectors are independent of the definition of the norm [6.7]. In contrast, the stretches $\{\sigma_j\}$, and the right/left principal axes depend on the choice of the norm. Appending them to dynamics destroys its invariance.

There is probably no name more liberally and more confusingly used in dynamical systems literature than that of Lyapunov (AKA Liapunov). Singular values / principal axes of strain tensor $J^\top J$ (objects natural to the theory of deformations) and their long-time limits can indeed be traced back to the thesis of Lyapunov [6.10, 6.8], and justly deserve sobriquet 'Lyapunov'. Oseledec [6.8] refers to them as 'Liapunov characteristic numbers', and Eckmann and Ruelle [6.11] as 'characteristic exponents'. The natural objects in dynamics are the linearized flow Jacobian matrix J^t, and its eigenvalues and eigenvectors (stability multipliers and covariant vectors). Why should they also be called 'Lyapunov'? The Jacobian matrix eigenvectors $\{\mathbf{e}^{(j)}\}$ (the covariant vectors) are often called 'covariant Lyapunov vectors', 'Lyapunov vectors', or 'stationary Lyapunov basis' [6.12] even though *they are not* the eigenvectors that correspond to the Lyapunov exponents. That's just confusing, for no good reason - the Lyapunov paper [6.10] is not about the linear stability Jacobian matrix J, it is about $J^\top J$ and the associated principal axes. However, Trevisan [6.7] refers to covariant vectors as 'Lyapunov vectors', and Radons [6.13] calls them 'Lyapunov modes', motivated by thinking of these eigenvectors as a generalization of 'normal modes' of mechanical systems, whereas by ith 'Lyapunov mode' Takeuchi and Chaté [6.14] mean $\{\lambda_j, \mathbf{e}^{(j)}\}$, the set of the ith stability exponent and the associated covariant vector. Kunihiro *et al.* [6.15] call the eigenvalues of stability matrix (4.3), evaluated at a given instant in time, the 'local Lyapunov exponents', and they refer to the set of stability exponents (4.8) for a finite time Jacobian matrix as the 'intermediate Lyapunov exponent', "averaged" over a finite time period. Then there is the unrelated, but correctly attributed 'Lyapunov equation' of control theory, which is the linearization of the 'Lyapunov function', and there is the 'Lyapunov orbit' of celestial mechanics, entirely unrelated to any of objects discussed above.

In short: we do not recommend that you evaluate Lyapunov exponents; compute stability exponents and the associated covariant vectors instead. Cost less and gets you

more insight. Whatever you call your exponents, please state clearly how are they being computed. While the Lyapunov exponents are a diagnostic for chaos, we are doubtful of their utility as means of predicting any observables of physical significance. This is the minority position - in the literature one encounters many provocative speculations, especially in the context of foundations of statistical mechanics ('hydrodynamic' modes) and the existence of a Lyapunov spectrum in the thermodynamic limit of spatiotemporal chaotic systems.

Remark 6.2 Matrix decompositions of the Jacobian matrix. A 'polar decomposition' of a matrix or linear operator is a generalization of the factorization of complex number into the polar form, $z = r\, \exp(\phi)$. Matrix polar decomposition is explained in refs. [6.16, 6.17, 6.18, 6.19]. One can go one step further than the polar decomposition (6.2) into a product of a rotation and a symmetric matrix by diagonalizing the symmetric matrix by a second rotation, and thus express any matrix with real elements in the singular value decomposition (SVD) form

$$J = R_1 D R_2{}^\top , \tag{6.13}$$

where D is diagonal and real, and R_1, R_2 are orthogonal matrices, unique up to permutations of rows and columns. The diagonal elements $\{\sigma_1, \sigma_2, \ldots, \sigma_d\}$ of D are the *singular values* of J.

Though singular values decomposition provides geometrical insights into how tangent dynamics acts, many popular algorithms for asymptotic stability analysis (computing Lyapunov spectrum) employ another standard matrix decomposition, the QR scheme [6.20], through which a nonsingular matrix J is (uniquely) written as a product of an orthogonal and an upper triangular matrix $J = QR$. This can be thought as a Gram-Schmidt decomposition of the column vectors of J. The geometric meaning of QR decomposition is that the volume of the d-dimensional parallelepiped spanned by the column vectors of J has a volume coinciding with the product of the diagonal elements of the triangular matrix R, whose role is thus pivotal in algorithms computing Lyapunov spectra [6.21].

Remark 6.3 Numerical evaluation of Lyapunov exponents. There are volumes of literature on numerical computation of the Lyapunov exponents, see for example refs. [6.22, 6.11, 6.23, 6.24]. For early numerical methods to compute Lyapunov vectors, see refs. [6.25, 6.26]. The drawback of the Gram-Schmidt method is that the vectors so constructed are orthogonal by fiat, whereas the stable / unstable eigenvectors of the Jacobian matrix are in general not orthogonal. Hence the Gram-Schmidt vectors are not covariant, i.e., the linearized dynamics does not transport them into the eigenvectors of the Jacobian matrix computed further downstream. For computation of covariant vectors, see refs. [6.27, 6.28].

6.3 Examples

The reader is urged to study the examples collected here. To return back to the main text, click on [click to return] pointer on the margin.

Example 6.1 ***Lyapunov exponent.*** *Given a 1-dimensional map, consider observable* $\lambda(x) = \ln|f'(x)|$ *and integrated observable*

$$A^n(x_0) = \sum_{k=0}^{n-1} \ln|f'(x_k)| = \ln\left|\prod_{k=0}^{n-1} f'(x_k)\right| = \ln\left|\frac{\partial f^n}{\partial x}(x_0)\right| .$$

The Lyapunov exponent is the average rate of the expansion

$$\lambda(x_0) = \lim_{n\to\infty} \frac{1}{n} \sum_{k=0}^{n-1} \ln|f'(x_k)| .$$

See sect. 6.2 for further details.

Example 6.2 ***Singular values and geometry of deformations:*** *Suppose we are in three dimensions, and the Jacobian matrix* J *is not singular (yet another confusing usage of word 'singular'), so that the diagonal elements of* D *in (6.13) satisfy* $\sigma_1 \geq \sigma_2 \geq \sigma_3 > 0$. *Consider how* J *maps the unit ball* $\mathcal{S} = \{x \in \mathrm{R}^3 \,|\, x^2 = 1\}$. V *is orthogonal (rotation/reflection), so* $V^\top\mathcal{S}$ *is still the unit sphere: then* D *maps* $\mathcal{S}$ *onto ellipsoid* $\tilde{\mathcal{S}} = \{y \in \mathrm{R}^3 \,|\, y_1^2/\sigma_1^2 + y_2^2/\sigma_2^2 + y_3^2/\sigma_3^2 = 1\}$ *whose principal axes directions - y coordinates - are determined by* V. *Finally the ellipsoid is further rotated by the orthogonal matrix* U. *The local directions of stretching and their images under* J *are called the right-hand and left-hand singular vectors for* J *and are given by the columns in* V *and* U *respectively: it is easy to check that* $Jv_k = \sigma_k u_k$, *if* v_k, u_k *are the k-th columns of* V *and* U. click to return: p. **??**

Exercises

6.1. **Principal stretches.** Consider $dx = f(x_0 + dx_0) - f(x_0)$, and show that $dx = Mdx_0 +$ higher order terms when $\|dx_0\| \ll 1$. (Hint: use Taylor expansion for a vector function.) Here, $\|dx_0\| \equiv \sqrt{dx_0 \cdot dx_0}$ is the norm induced by the usual Euclidean dot (inner) product. Then let $dx_0 = (d\ell)e_i$ and show that $\|dx_0\| = d\ell$ and $\|dx\| = \sigma_i d\ell$. (Christov *et al.* [2.1])

6.2. **Eigenvalues of the Cauchy-Green strain tensor.** Show that $\kappa_i = \sigma_i^2$ using the definition of C, the polar decomposition theorem, and the properties of eigenvalues. (Christov *et al.* [2.1])

6.3. **How unstable is the Hénon attractor?**

(a) Evaluate numerically the Lyapunov exponent λ by iterating some 100,000 times or so the Hénon map

$$\begin{bmatrix} x' \\ y' \end{bmatrix} = \begin{bmatrix} 1 - ax^2 + y \\ bx \end{bmatrix}$$

for $a = 1.4$, $b = 0.3$.

(b) Would you describe the result as a 'strange attractor'? Why?

(c) How robust is the Lyapunov exponent for the Hénon attractor? Evaluate numerically the Lyapunov exponent by iterating the Hénon map for $a = 1.39945219$, $b = 0.3$. How much do you now trust your result for part (a) of this exercise?

(d) Re-examine this computation by plotting the iterates, and erasing the plotted points every 1000 iterates or so. Keep at it until the 'strange' attractor vanishes like the smile of the Chesire cat. What replaces it? Do a few numerical experiments to estimate the length of typical transient before the dynamics settles into this long-time attractor.

(e) Use your Newton search routine to confirm existence of this attractor. Compute its Lyapunov exponent, compare with your numerical result from above. What is the itinerary of the attractor.

(f) Would you describe the result as a 'strange attractor'? Do you still have confidence in claims such as the one made for the part (b) of this exercise?

6.4. **Rössler attractor Lyapunov exponents.**

(a) Evaluate numerically the expanding Lyapunov exponent λ_e of the Rössler attractor (2.23).

(b) Plot your own version of figure 6.3. Do not worry if it looks different, as long as you understand why your plot looks the way it does. (Remember the nonuniform contraction/expansion of figure 4.3.)

(c) Give your best estimate of λ_e. The literature gives surprisingly inaccurate estimates - see whether you can do better.

(d) Estimate the contracting Lyapunov exponent λ_c. Even though it is much smaller than λ_e, a glance at the stability matrix (4.30) suggests that you can probably get it by integrating the infinitesimal volume along a long-time trajectory, as in (4.29).

References

[6.1] I. Goldhirsch, P. L. Sulem, and S. A. Orszag, Stability and Lyapunov stability of dynamical systems: A differential approach and a numerical method, Physica D **27**, 311 (1987).

[6.2] E. N. Lorenz, A study of the predictability of a 28-variable atmospheric model, Tellus **17**, 321 (1965).

[6.3] E. N. Lorenz, Irregularity: a fundamental property of the atmosphere*, Tellus A **36**, 98 (1984).

[6.4] S. Yoden and M. Nomura, Finite-time Lyapunov stability analysis and its application to atmospheric predictability, J. Atmos. Sci. **50**, 1531 (1993).

[6.5] W. G. Hoover and C. G. Hoover, Local Gram–Schmidt and covariant Lyapunov vectors and exponents for three harmonic oscillator problems, Commun. Nonlinear Sci. Numer. Simul. **17**, 1043 (2012), `arXiv:1106.2367`.

[6.6] J. M. Greene and J.-S. Kim, The calculation of Lyapunov spectra, Physica D **24**, 213 (1987).

[6.7] A. Trevisan and F. Pancotti, Periodic orbits, Lyapunov vectors, and singular vectors in the Lorenz system, J. Atmos. Sci. **55**, 390 (1998).

[6.8] V. I. Oseledec, A multiplicative ergodic theorem. Liapunov characteristic numbers for dynamical systems, Trans. Moscow Math. Soc. **19**, 197 (1968).

[6.9] M. Pollicott, *Lectures on Ergodic Theory and Pesin Theory in Compact Manifolds*, (Cambridge Univ. Press, Cambridge 1993).

[6.10] A. Lyapunov, Problème général de la stabilité du mouvement, Ann. of Math. Studies **17** (1977), Russian original Kharkow, 1892.

[6.11] J.-P. Eckmann and D. Ruelle, Ergodic theory of chaos and strange attractors, Rev. Mod. Phys. **57**, 617 (1985).

[6.12] S. V. Ershov and A. B. Potapov, On the concept of stationary Lyapunov basis, Physica D **118**, 167 (1998).

[6.13] H. Yang and G. Radons, Comparison between covariant and orthogonal Lyapunov vectors, Phys. Rev. E **82**, 046204 (2010), arXiv:1008.1941.

[6.14] K. A. Takeuchi and H. Chaté, Collective Lyapunov modes, 2012, arXiv:1207.5571.

[6.15] T. Kunihiro *et al.*, Chaotic behavior in classical Yang-Mills dynamics, Phys. Rev. D **82**, 114015 (2010).

[6.16] J. M. Ottino, *The Kinematics of Mixing: Stretching, Chaos and Transport* (Cambridge Univ. Press, Cambridge, 1989).

[6.17] C. Truesdell, *A First Course in Rational Continuum Mechanics: General concepts* Vol. 1 (Academic Press, New York, 1991).

[6.18] M. E. Gurtin, *An Introduction to Continuum Mechanics* (Academic Press, New York, 1981).

[6.19] R. A. Horn and C. R. Johnson, *Matrix Analysis* (Cambridge Univ. Press, Cambridge, 1990).

[6.20] C. Meyer, *Matrix Analysis and Applied Linear Algebra* (SIAM, Philadelphia, 2000).

[6.21] C. Skokos, The Lyapunov characteristic exponents and their computation, p. 63 (2010), arXiv:0811.0882.

[6.22] A. Wolf, J. B. Swift, H. L. Swinney, and J. A. Vastano, Determining Lyapunov exponents from a time series, Physica D **16**, 285 (1985).

[6.23] J.-P. Eckmann, S. O. Kamphorst, D. Ruelle, and S. Ciliberto, Liapunov exponents from time series, Phys. Rev. A **34**, 4971 (1986).

[6.24] J.-L. Thiffeault, Derivatives and constraints in chaotic flows: asymptotic behaviour and a numerical method, Physica D **172**, 139 (2002), arXiv:nlin/0101012.

[6.25] I. Shimada and T. Nagashima, A numerical approach to ergodic problem of dissipative dynamical systems, Prog. Theor. Phys. **61**, 1605 (1979).

[6.26] G. Benettin, L. Galgani, A. Giorgilli, and J. M. Strelcyn, Lyapunov characteristic exponents for smooth dynamical systems; a method for computing all of them. Part 1: theory, Meccanica **15**, 9 (1980).

[6.27] F. Ginelli *et al.*, Characterizing dynamics with covariant Lyapunov vectors, Phys. Rev. Lett. **99**, 130601 (2007), arXiv:0706.0510.

[6.28] A. Politi, A. Torcini, and S. Lepri, Lyapunov exponents from node-counting arguments, J. Phys. IV **8**, 263 (1998).

Chapter 6A

Fixed points

HAVING SET UP the dynamical context, we now turn to the key and unavoidable numerical task in this subject; we must search for the solutions (x, T), $x \in \mathbb{R}^d_+$, $T \in \mathbb{R}$ satisfying the *periodic orbit condition*

$$f^{t+T}(x) = f^t(x), \qquad T > 0 \tag{6A.14}$$

for a given flow or map.

Sadly, searching for periodic orbits will never become as popular as a week on Côte d'Azur, or publishing yet another log-log plot in *Phys. Rev. Letters*. This chapter is the first of the series of hands-on guides to extraction of periodic orbits, and should be skipped on first reading - you can return to it whenever the need for finding actual cycles arises. A serious cyclist will ask "Where are the cycles? And what if they are long?" and read chapter 13. She will want to also learn about the variational methods to find cycles, and read chapter 29.

chapter 13

chapter 29

fast track:
chapter 14, p. 301

A *prime* cycle p of period T_p is a single traversal of the periodic orbit, so our task will be to find a periodic point $x \in \mathcal{M}_p$ and the shortest time T_p for which (13.1) has a solution. A periodic point of a flow f^t crossing a Poincaré section n times is a fixed point of P^n, the nth iterate of P, the return map (3.1); hence, we shall refer to all cycles as "fixed points" in this chapter. By cyclic invariance, Floquet multipliers and the period of the cycle are independent of the choice of the initial point, so it will suffice to solve (13.1) at a single periodic point.

section 5.3

If the cycle is an attracting limit cycle with a sizable basin of attraction, it can be found by integrating the flow for a sufficiently long time. If the cycle is unstable, simple integration forward in time will not reveal it, and the methods to be described here need to be deployed. In essence, any method for finding a cycle is based on devising a new dynamical system which possesses the same cycle, but for which this cycle is attractive. Beyond that, there is a great freedom in constructing such systems, and many different methods are used in practice.

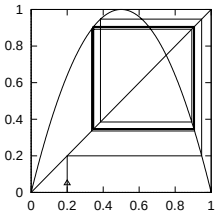

Figure 6A.4: The inverse time path to the $\overline{01}$-cycle of the logistic map $f(x) = 4x(1-x)$ from an initial guess of $x = 0.2$. At each inverse iteration we chose the 0 (respectively 1) branch.

6A.4 One-dimensional maps

So far we have given some qualitative hints for how to set out on a periodic orbit hunt. In what follows, we teach you how to nail down periodic orbits numerically.

(F. Christiansen)

6A.4.1 Inverse iteration

Let us first consider a very simple method to find the unstable cycles of a 1-dimensional map such as the logistic map. Unstable cycles of 1-dimensional maps are attracting cycles of the inverse map. The inverse map is not single-valued, so at each backward iteration we have a choice of branch to make. By choosing the branch according to the symbolic dynamics of the cycle we are trying to find, we will automatically converge to the desired cycle. The rate of convergence is given by the stability of the cycle, i.e., the convergence is exponentially fast. Figure 6A.4 shows such a path to the $\overline{01}$-cycle of the logistic map.

exercise 13.10

The method of inverse iteration is fine for finding cycles for 1-d maps and some 2-dimensional systems such as the repeller of exercise 13.10. It is not particularly fast, however, especially if the inverse map is not known analytically. It also completely fails for higher dimensional systems where we have both stable and unstable directions. Inverse iteration will exchange these, but we will still be left with both stable and unstable directions. The best strategy is to directly attack the problem of finding solutions of $f^T(x) = x$.

6A.4.2 Newton method

Newton method for determining a zero x^* of a function $F(x)$ of one variable is based on a linearization around a starting guess x_0:

$$F(x) \approx F(x^{(0)}) + F'(x^{(0)})(x - x^{(0)}). \tag{6A.15}$$

An approximate solution $x^{(1)}$ of $F(x) = 0$ is

$$x^{(1)} = x^{(0)} - F(x^{(0)})/F'(x^{(0)}). \tag{6A.16}$$

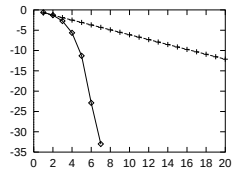

Figure 6A.5: Convergence of Newton method ($\diamond$) vs. inverse iteration (+). The error after n iterations searching for the $\overline{01}$-cycle of the logistic map $f(x) = 4x(1-x)$ with an initial starting guess of $x_1 = 0.2, x_2 = 0.8$. The y-axis is $\log_{10}$ of the error. The difference between the exponential convergence of the inverse iteration method and the super-exponential convergence of Newton method is dramatic.

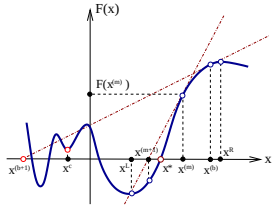

Figure 6A.6: Newton method: bad initial guess $x^{(b)}$ leads to the Newton estimate $x^{(b+1)}$ far away from the desired zero of $F(x)$. Sequence $\cdots, x^{(m)}, x^{(m+1)}, \cdots$, starting with a good guess converges super-exponentially to x^*. The method diverges if it iterates into the basin of attraction of a local minimum x^c.

The approximate solution can then be used as a new starting guess in an iterative process. A fixed point of a map f is a solution to $F(x) = x - f(x) = 0$. We determine x by iterating

$$\begin{aligned} x^{(m)} &= g(x^{(m-1)}) = x^{(m-1)} - F(x^{(m-1)})/F'(x^{(m-1)}) \\ &= x^{(m-1)} - \frac{1}{1 - f'(x^{(m-1)})}(x^{(m-1)} - f(x^{(m-1)}))\,. \end{aligned} \tag{6A.17}$$

Provided that the fixed point is not marginally stable, $f'(x) \neq 1$ at the fixed point x, a fixed point of f is a super-stable fixed point of the Newton-Raphson map g, $g'(x) = 0$, and with a sufficiently good initial guess, the Newton-Raphson iteration will converge super-exponentially fast.

To illustrate the efficiency of Newton method we compare it to the inverse iteration method in figure 6A.5. Newton method wins hands down: the number of significant digits of the accuracy of the x estimate typically doubles with each iteration.

In order to avoid jumping too far from the desired x^* (see figure 6A.6), one often initiates the search by the *damped Newton method*,

$$\Delta x^{(m)} = x^{(m+1)} - x^{(m)} = -\frac{F(x^{(m)})}{F'(x^{(m)})}\Delta\tau\,, \qquad 0 < \Delta\tau \leq 1\,,$$

takes small $\Delta\tau$ steps at the beginning, reinstating to the full $\Delta\tau = 1$ jumps only when sufficiently close to the desired x^*.

example 6A.3 p. 128

6A.5 Flows

(R. Paškauskas and P. Cvitanović)

For a continuous time flow the periodic orbit the Floquet multiplier (5.12) along the flow direction always equals unity; the separation of any two points along a cycle remains unchanged after a completion of the cycle. More unit Floquet multipliers arise if the flow satisfies conservation laws, such as the symplectic invariance for Hamiltonian flows, or the dynamics is equivariant under a continuous symmetry transformation.

section 5.3.1

section 10.3

Let us apply the Newton method of (6A.16) to search for periodic orbits with unit Floquet multipliers, starting with the case of a *continuous time flow*. Assume that the periodic orbit condition (13.1) holds for $x+\Delta x$ and $T+\Delta t$, with the initial guesses x and T close to the desired solution, i.e., with $|\Delta x|$, Δt small. The Newton setup (6A.16)

$$\begin{aligned} 0 &= x+\Delta x - f^{T+\Delta t}(x+\Delta x) \\ &\approx x - f^T(x) + (1-J(x))\cdot\Delta x - v(f^T(x))\Delta t \end{aligned} \tag{6A.18}$$

suffers from two shortcomings. First, we now need to solve not only for the periodic point x, but for the period T as well. Second, the marginal, unit Floquet multiplier (5.12) along the flow direction (arising from the time-translation invariance of a periodic orbit) renders the factor $(1-J)$ in (6A.17) non-invertible: if x is close to the solution, $f^T(x)\approx x$, then $J(x)\cdot v(x) = v(f^T(x))\approx v(x)$. If Δx is parallel to the velocity vector, the derivative term $(1-J)\cdot\Delta x\approx 0$, and it becomes harder to invert $(1-J)$ as the iterations approach the solution.

As a periodic orbit p is a 1-dimensional set of points invariant under dynamics, Newton guess is not improved by picking Δx such that the new point lies on the orbit of the initial one, so we need to constrain the variation Δx to directions transverse to the flow, by requiring, for example, that

$$v(x)\cdot\Delta x = 0\,. \tag{6A.19}$$

Combining this constraint with the variational condition (6A.18) we obtain a Newton setup for flows, best displayed in the matrix form:

$$\begin{pmatrix} 1-J(x) & -v(x) \\ v(x) & 0 \end{pmatrix}\begin{pmatrix} \Delta x \\ \Delta t \end{pmatrix} = -\begin{pmatrix} x-f(x) \\ 0 \end{pmatrix} \tag{6A.20}$$

This illustrates the general strategy for determining periodic orbits in presence of continuous symmetries - for each symmetry, pick a point on the orbit by imposing a constraint, and compute the value of the corresponding continuous parameter (here the period T) by iterating the enlarged set of Newton equations. Constraining

the variations to transverse ones thus fixes both of Newton's shortcomings: it breaks the time-translation invariance, and the period T can be read off once the fixed point has been found (hence we omit the superscript in f^T for the remainder of this discussion).

More generally, the Poincaré surface of section technique of sect. 3.1 turns the periodic orbit search into a fixed point search on a suitably defined surface of section, with a neighboring point variation Δx with respect to a reference point x constrained to *stay* on the surface manifold (3.2),

$$U(x+\Delta x) = U(x) = 0\,. \tag{6A.21}$$

The price to pay are constraints imposed by the section: in order to *stay* on the surface, arbitrary variation Δx is not allowed.

example 6A.4 p. 129

Résumé

There is no general computational algorithm that is guaranteed to find all solutions (up to a given period $T_{\rm max}$) to the periodic orbit condition

$$f^{t+T}(x) = f^t(x)\,, \qquad T>0$$

for a general flow or mapping. Due to the exponential divergence of nearby trajectories in chaotic dynamical systems, direct solution of the periodic orbit condition can be numerically very unstable.

With a sufficiently good initial guess, the Newton-Raphson formula

$$\begin{pmatrix} 1-J & -v(x) \\ a & 0 \end{pmatrix}\begin{pmatrix} \delta x \\ \delta T \end{pmatrix} = \begin{pmatrix} f(x)-x \\ 0 \end{pmatrix}$$

yields improved estimate $x' = x+\delta x, T' = T+\delta T$. Iteration then yields the period T and the location of a periodic point x_p in the Poincaré section $(x_p - x_0)\cdot a = 0$, where a is a vector normal to the Poincaré section at x_0.

Commentary

Remark 6A.4 Piecewise linear maps. The Lozi map (3.19) is linear, and hundred of thousands of cycles can easily be computed by [2×2] matrix multiplication and inversion.

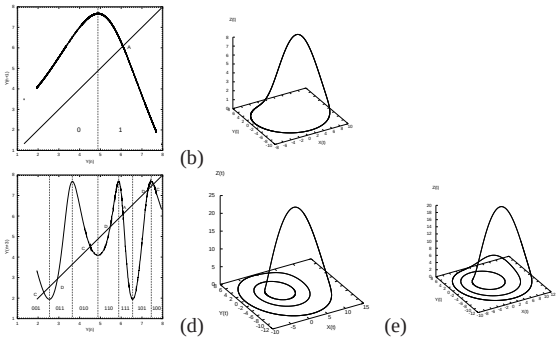

Figure 6A.7: (a) The $y \to P_1(y,z)$ return map for the $x = 0$, $y > 0$ Poincaré section of the Rössler flow figure 2.6. (b) The $\overline{1}$-cycle found by taking the fixed point $y_{k+n} = y_k$ together with the fixed point of the $z \to z$ return map (not shown) as an initial guess $(0, y^{(0)}, z^{(0)})$ for the Newton-Raphson search. (c) The third iterate, $y_{k+3} = P_1^3(y_k, z_k)$, of the Poincaré return map (3.1) together with the corresponding plot for $z_{k+3} = P_2^3(y_k, z_k)$, is used to pick initial guesses for the Newton-Raphson searches for the two 3-cycles: (d) the $\overline{001}$ cycle, and (e) the $\overline{011}$ cycle. (G. Simon)

Remark 6A.5 Newton gone wild. Skowronek and Gora [6A.22] offer an interesting discussion of Newton iterations gone wild while searching for roots of polynomials as simple as $x^2 + 1 = 0$.

6A.6 Examples

Example 6A.3 ***Rössler attractor.*** *We run a long simulation of the Rössler flow f^t, plot a Poincaré section, as in figure 3.2, and extract the corresponding Poincaré return map P, as in figure 3.3. Luck is with us, since figure 6A.7 (a) return map $y \to P_1(y,z)$ is quite reminiscent of a parabola, we take the unimodal map symbolic dynamics, sect. 11.3, as our guess for the covering dynamics. Strictly speaking, the attractor is "fractal," but for all practical purposes the return map is 1-dimensional; your printer will need a resolution better than 10^{14} dots per inch to even begin resolving its structure.*

Periodic points of a prime cycle p of cycle length n_p for the $x = 0$, $y > 0$ Poincaré section of the Rössler flow figure 2.6 are fixed points $(y,z) = P^n(y,z)$ of the nth Poincaré return map.

Using the fixed point $y_{k+1} = y_k$ in figure 6A.7 (a) together with the simultaneous fixed point of the $z \to P_1(y,z)$ return map (not shown) as a starting guess $(0, y^{(0)}, z^{(0)})$ for the Newton-Raphson search for the cycle p with symbolic dynamics label $\overline{1}$, we find the cycle figure 6A.7 (b) with the Poincaré section point $(0, y_p, z_p)$, period T_p, expanding, marginal, contracting Floquet multipliers $(\Lambda_{p,e}, \Lambda_{p,m}, \Lambda_{p,c})$, and the corresponding Lyapunov exponents $(\lambda_{p,e}, \lambda_{p,m}, \lambda_{p,c})$: exercise 13.7

$$
\begin{aligned}
\overline{1}\text{-cycle:} \quad (x,y,z) &= (0, 6.09176832, 1.2997319) \\
T_1 &= 5.88108845586 \\
(\Lambda_{1,e}, \Lambda_{1,m}, \Lambda_{1,c}) &= (-2.40395353, 1 + 10^{-14}, -1.29 \times 10^{-14}) \\
(\lambda_{1,e}, \lambda_{1,m}, \lambda_{1,c}) &= (0.149141556, 10^{-14}, -5.44)\,. \qquad \text{(6A.22)}
\end{aligned}
$$

The Newton-Raphson method that we used is described in sect. 6A.5.

As an example of a search for longer cycles, we use $y_{k+3} = P_1^3(y_k, z_k)$, the third iterate of the Poincaré return map (3.1) plotted in figure 6A.7 (c), together with a corresponding plot for $z_{k+3} = P_2^3(y_k, z_k)$, to pick starting guesses for the Newton-Raphson searches for the two 3-cycles plotted in figure 6A.7 (d), (e). For a listing of the short cycles of the Rössler flow, consult exercise 13.7.

The numerical evidence suggests (though a proof is lacking) that all cycles that comprise the strange attractor of the Rössler flow are hyperbolic, each with an expanding eigenvalue $|\Lambda_e| > 1$, a contracting eigenvalue $|\Lambda_c| < 1$, and a marginal eigenvalue $|\Lambda_m| = 1$ corresponding to displacements along the direction of the flow.

For the Rössler flow the contracting eigenvalues turn out to be insanely contracting, a factor of e^{-32} per one par-course of the attractor, so their numerical determination is quite difficult. Fortunately, they are irrelevant; for all practical purposes the strange attractor of the Rössler flow is 1-dimensional, a very good realization of a horseshoe template. (G. Simon and P. Cvitanović) cont'd return: p. ??

Example 6A.4 ***A hyperplane Poincaré section.*** *Let us for the sake of simplicity assume that the Poincaré surface of section is a (hyper)-plane, i.e., it is given by the linear condition (3.14)*

$$(x - x_0) \cdot \hat{n} = 0, \qquad \text{(6A.23)}$$

where $\hat{n}$ is a vector normal to the Poincaré section and x_0 is any point in the Poincaré section. The Newton setup is then (derived as (6A.20))

$$\begin{pmatrix} 1 - J & -v(x) \\ \hat{n} & 0 \end{pmatrix} \begin{pmatrix} x' - x \\ \Delta t \end{pmatrix} = \begin{pmatrix} -F(x) \\ 0 \end{pmatrix}. \qquad \text{(6A.24)}$$

The last row in this equation ensures that x will be in the surface of section, and the addition of $v(x)\Delta t$, a small vector along the direction of the flow, ensures that such an x can be found, at least if x is sufficiently close to a fixed point of f. Alternatively, this can be solved a least squares problem.

To illustrate that the addition of the extra constraint resolves the problem of $(1 - J)$ non-invertability, we consider the particularly simple example of a 3-d flow with the $(x, y, 0)$-plane as the Poincaré section, $a = (0, 0, 1)$. Let all trajectories cross the Poincaré section perpendicularly, so that $v = (0, 0, v_z)$, which means that the marginally stable direction is also perpendicular to the Poincaré section. Furthermore, let the unstable direction be parallel to the x-axis and the stable direction be parallel to the y-axis. The Newton setup is now

$$\begin{pmatrix} 1 - \Lambda_u & 0 & 0 & 0 \\ 0 & 1 - \Lambda_s & 0 & 0 \\ 0 & 0 & 0 & -v_z \\ 0 & 0 & 1 & 0 \end{pmatrix} \begin{pmatrix} \delta_x \\ \delta_y \\ \delta_z \\ \delta\tau \end{pmatrix} = \begin{pmatrix} -F_x \\ -F_y \\ -F_z \\ 0 \end{pmatrix}. \qquad \text{(6A.25)}$$

If one considers only the upper-left [3 × 3] matrix (which we started out with, prior to adding the constraint (6A.23)) then this matrix is not invertible and the equation does not have a unique solution. However, the full [4×4] matrix is invertible, as $\det(\cdot) = -v_z \det(1 - M_\perp)$, *where $M_\perp$ is the* $[2 \times 2]$ monodromy matrix *for a surface of section transverse to the orbit (see sect. 5.5).* (F. Christiansen) cont'd return: p. ??

Exercises

6A.1. **Ulam map periodic points.** (continued from exercise 11.8)

(a) compute the five periodic points of cycle $\overline{10011}$ for the Ulam map (11.5) $f(x) = 4x(1-x)$. using your Newton or other routine.

(b) compute the five periodic points of cycle $\overline{10000}$

(c) plot the above two cycles on the graph of the Ulam map, verify that their topological ordering is as in the 'canonical' full tent map exercise 11.8.

(d) (optional) This works only for the Ulam map: compute periodic points by conjugating the full tent map periodic points of exercise 11.8 using exercise B.4.

6A.2. **Cycles stabilities for the Ulam map (exact).** In exercise 6A.1 you should have observed that the numerical results for the cycle Floquet multipliers (4.42) are exceptionally simple: the Floquet multiplier of the $x_0 = 0$ fixed point is 4, while the eigenvalue of any other n-cycle is $\pm 2^n$. Prove this. (Hint: the Ulam map can be conjugated to the tent map (11.4). This problem is perhaps too hard, but give it a try - the answer is in many introductory books on nonlinear dynamics.)

6A.3. **Cycle stability.** Add to the pinball simulator of exercise 8.1 a routine that evaluates the expanding eigenvalue for a given cycle.

6A.4. **Pinball cycles.** Determine the stability and length of all fundamental domain prime cycles of the binary symbol string lengths up to 5 (*or longer*) for $R : a = 6$ 3-disk pinball.

6A.5. **Newton-Raphson method.** Implement the Newton-Raphson method in 2-dimensional and apply it to the determination of pinball cycles.

6A.6. **Fundamental domain fixed points.** Use the formula (8.11) for billiard Jacobian matrix to compute the periods T_p and the expanding eigenvalues Λ_p of the fundamental domain $\overline{0}$ (the 2-cycle of the complete 3-disk space) and $\overline{1}$ (the 3-cycle of the complete 3-disk space) fixed points:

	T_p	Λ_p
$\overline{0}$:	$R-2$	$R-1+R\sqrt{1-2/R}$
$\overline{1}$:	$R-\sqrt{3}$	$-\frac{2R}{\sqrt{3}}+1-\frac{2R}{\sqrt{3}}\sqrt{1-\sqrt{3}/R}$

(6A.26)

We have set the disk radius to $a = 1$.

6A.7. **Fundamental domain 2-cycle.** Verify that for the $\overline{10}$-cycle the cycle length and the trace of the Jacobian matrix are given by

$$\begin{aligned} L_{10} &= 2\sqrt{R^2-\sqrt{3}R+1}-2, \\ \operatorname{tr}\mathbf{J}_{10} &= \Lambda_{10}+1/\Lambda_{10} \\ &= 2L_{10}+2+\frac{1}{2}\,\frac{L_{10}(L_{10}+2)^2}{\sqrt{3}R/2-1}\ . \end{aligned} \tag{6A.27}$$

The $\overline{10}$-cycle is drawn in figure 12.12. The unstable eigenvalue Λ_{10} follows from (7.30).

6A.8. **A test of your pinball simulator: $\overline{10}$-cycle.** Test your exercise 8.4 pinball simulator stability evaluation by checking numerically the exact analytic $\overline{10}$-cycle stability formula (13.14).

6A.9. **Rössler flow cycles.** (continuation of exercise 4.4) Determine all cycles for the Rössler flow (2.23), as well as their stabilities, up to

(a) 3 Poincaré section returns

(b) (optional) 5 Poincaré section returns (Hint: implement (6A.24), the multipoint shooting methods for flows; you can cross-check your shortest cycles against the ones listed in the table.)

Table: *The Rössler flow (2.23): The itinerary p, a periodic point $x_p = (0, y_p, z_p)$ and the expanding eigenvalue Λ_p for all cycles up to topological length 7.*
(J. Mathiesen, G. Simon, A. Basu)

n_p	p	y_p	z_p	Λ_e
1	1	6.091768	1.299732	-2.403953
2	01	3.915804	3.692833	-3.512007
3	001	2.278281	7.416481	-2.341923
	011	2.932877	5.670806	5.344908
4	0111	3.466759	4.506218	-16.69674
5	01011	4.162799	3.303903	-23.19958
	01111	3.278914	4.890452	36.88633
6	001011	2.122094	7.886173	-6.857665
	010111	4.059211	3.462266	61.64909
	011111	3.361494	4.718206	-92.08255
7	0101011	3.842769	3.815494	77.76110
	0110111	3.025957	5.451444	-95.18388
	0101111	4.102256	3.395644	-142.2380
	0111111	3.327986	4.787463	218.0284

6A.10. **Cycle stability, helium.** Add to the helium integrator of exercise 2.10 a routine that evaluates the expanding eigenvalue for a given cycle.

6A.11. **Colinear helium cycles.** Determine the stability and length of all fundamental domain prime cycles up to symbol sequence length 5 or longer for collinear helium of figure 7.2.

6A.12. **Uniqueness of unstable cycles***.** Prove that there exists only one 3-disk prime cycle for a given finite admissible prime cycle symbol string. Hints: look at the Poincaré maps; can you show that there is exponential contraction to a unique periodic point with a given itinerary? Exercise 29.1 might be helpful in this effort.

6A.13. **Inverse iteration method for a Hénon repeller.**

Table: *All periodic orbits up to 6 bounces for the Hamiltonian Hénon map (6A.28) with $a = 6$. Listed are the cycle itinerary, its expanding eigenvalue Λ_p, and its "center of mass." The "center of mass" is listed because it turns out that it is often a simple rational or a quadratic irrational.*

p	Λ_p	$\sum x_{p,i}$
0	0.715168×10^{1}	-0.607625
1	-0.295285×10^{1}	0.274292
10	-0.989898×10^{1}	0.333333
100	-0.131907×10^{3}	-0.206011
110	0.558970×10^{2}	0.539345
1000	-0.104430×10^{4}	-0.816497
1100	0.577998×10^{4}	0.000000
1110	-0.103688×10^{3}	0.816497
10000	-0.760653×10^{4}	-1.426032
11000	0.444552×10^{4}	-0.606654
10100	0.770202×10^{3}	0.151375
11100	-0.710688×10^{3}	0.248463
11010	-0.589499×10^{3}	0.870695
11110	0.390994×10^{3}	1.095485
100000	-0.545745×10^{5}	-2.034134
110000	0.322221×10^{5}	-1.215250
101000	0.513762×10^{4}	-0.450662
111000	-0.478461×10^{4}	-0.366025
110100	-0.639400×10^{4}	0.333333
101100	-0.639400×10^{4}	0.333333
111100	0.390194×10^{4}	0.548583
111010	0.109491×10^{4}	1.151463
111110	-0.104338×10^{4}	1.366025

Consider the Hénon map (3.17) for the area-preserving ("Hamiltonian") parameter value $b = -1$. The coordinates of a periodic orbit of length n_p satisfy the equation

$$x_{p,i+1} + x_{p,i-1} = 1 - a x_{p,i}^2\,, \quad i = 1, ..., n_p\,, \tag{6A.28}$$

with the periodic boundary condition $x_{p,0} = x_{p,n_p}$. Verify that the itineraries and the stabilities of the short periodic orbits for the Hénon repeller (6A.28) at $a = 6$ are as listed above.

Hint: you can use any cycle-searching routine you wish, but for the complete repeller case (all binary sequences are realized), the cycles can be evaluated simply by inverse iteration, using the inverse of (6A.28)

$$x''_{p,i} = S_{p,i}\sqrt{\frac{1-x'_{p,i+1}-x'_{p,i-1}}{a}},\quad i = 1, ..., n_p\,.$$

Here $S_{p,i}$ are the signs of the corresponding periodic point coordinates, $S_{p,i} = x_{p,i}/|x_{p,i}|$. (G. Vattay)

6A.14. **Newton setups for flows.**

(a) We have formulated three Newton setups for flows: the 'local' setup (6A.20), the 'hyperplane' setup (6A.24), and the 'global' setup (13.8). Derive (13.8) and verify that if the surface of section is a hyperplane, it reduces to (6A.24). (Hint: it is not inconceivable that (6A.24) is wrong as it stands.)

(b) (optional) Derive (13.10), the Newton setup for Hamiltonian flows.

6A.15. **"Center of mass" puzzle**.** Why is the "center of mass," tabulated in exercise 6A.13, often a rational number?

References

[6A.1] D. Auerbach, P. Cvitanović, J.-P. Eckmann, G.H. Gunaratne and I. Procaccia, *Phys. Rev. Lett.* **58**, 2387 (1987).

[6A.2] M. Baranger and K.T.R. Davies *Ann. Physics* **177**, 330 (1987).

[6A.3] B.D. Mestel and I. Percival, *Physica D* **24**, 172 (1987); Q. Chen, J.D. Meiss and I. Percival, *Physica D* **29**, 143 (1987).

[6A.4] find Helleman et all Fourier series methods

[6A.5] J.M. Greene, *J. Math. Phys.* **20**, 1183 (1979)

[6A.6] P.H. Richter, H.-J. Scholz and A. Wittek, "A breathing chaos," *Nonlinearity* **1**, 45 (1990).

[6A.7] H.E. Nusse and J. Yorke, "A procedure for finding numerical trajectories on chaotic saddles" *Physica* **D 36**, 137 (1989).

[6A.8] D.P. Lathrop and E.J. Kostelich, "Characterization of an experimental strange attractor by periodic orbits" *Phys. Rev. A* **40**, 4028 (1989).

[6A.9] T. E. Huston, K.T.R. Davies and M. Baranger *Chaos* **2**, 215 (1991).

[6A.10] M. Brack, R. K. Bhaduri, J. Law and M. V. N. Murthy, *Phys. Rev. Lett.* **70**, 568 (1993).

[6A.11] C. Polymilis, G. Servizi, Ch. Skokos, G. Turchetti, and M. N. Vrahatis, "Locating periodic orbits by Topological Degree theory;" arXiv:nlin.CD/0211044.

[6A.12] B. Doyon and L. J. Dubé, "On Jacobian matrices for flows," *CHAOS* **15**, 013108 (2005).

[6A.13] S.C. Farantos, "Exploring Molecular Vibrational Motions with Periodic Orbits," *Int. Rev. Phys. Chem.* **15**, 345 (1996); tccc.iesl.forth.gr/~farantos, tccc.iesl.forth.gr/articles/review/review1.ps.gz.

[6A.14] S.C. Farantos, "POMULT: A Program for Computing Periodic Orbits in Hamiltonian Systems Based on Multiple Shooting Algorithms," *Computer Phys. Comm.* **108**, 240 (1998); esperia.iesl.forth.gr/~farantos/articles/po_cpc/po_ccp.ps.

[6A.15] M. Baranger, K.T.R. Davies and J.H. Mahoney, "The calculation of periodic trajectories," *Ann. Phys.* **186**, 95 (1988).

[6A.16] K.T.R. Davies, T.E. Huston and M. Baranger, "Calculations of periodic trajectories for the Henon-Heiles Hamiltonian using the monodromy method," *CHAOS* **2**, 215 (1992).

[6A.17] N.S. Simonović, "Calculations of periodic orbits: The monodromy method and application to regularized systems," *CHAOS* **9**, 854 (1999).

[6A.18] N.S. Simonović, "Calculations of Periodic Orbits for Hamiltonian Systems with Regularizable Singularities," *Few-Body-Systems* **32**, 183 (2003).

[6A.19] Z. Gills, C. Iwata, R. Roy, I.B. Scwartz and I. Triandaf, "Tracking Unstable Steady States: Extending the Stability Regime of a Multimode Laser System," *Phys. Rev. Lett.* **69**, 3169 (1992).

[6A.20] N.J. Balmforth, P. Cvitanović, G.R. Ierley, E.A. Spiegel and G. Vattay, "Advection of vector fields by chaotic flows," *Stochastic Processes in Astrophysics, Annals of New York Academy of Sciences* **706**, 148 (1993); preprint.

[6A.21] A. Endler and J.A.C. Gallas, "Rational reductions of sums of orbital coordinates for a Hamiltonian repeller," (2005).

[6A.22] L. Skowronek and P. F. Gora, "Chaos in Newtonian iterations: Searching for zeros which are not there," Acta Phys. Polonica B **38**, 1909 (2007); arXiv:nlin.CD/0703061.